Featured in Physics

Reconstructing grain-shape statistics from electron back-scatter diffraction microscopy

R. S. Farr[*]

Jacobs Douwe Egberts, Banbury, Oxfordshire, OX16 2QU, United Kingdom
and London Institute for Mathematical Sciences, 35a South Street, Mayfair, W1K 2XF, United Kingdom

Z. Vukmanovic[†] and M. B. Holness[‡]
Department of Earth Sciences, University of Cambridge, CB2 3EQ, United Kingdom

E. Griffiths
297 Sandy Bay Road, Sandy Bay, Tasmania, Australia

Reconstructing the three-dimensional (3D) size and shape distribution of randomly oriented grains using only images of cross sections remains an important challenge. Even for ellipsoids, a solution is only possible when they are solids of revolution, and may still be numerically unstable. Here we show that crystallographic orientation data, for example from electron back-scatter diffraction (EBSD), provides enough additional information to obtain moments of the 3D grain distribution, provided grain shapes can be assumed to align with crystal axes. We show that this moment method can give an average 3D grain size and shape (with error estimate) which is rigorous for ellipsoids and a good approximation for cuboidal grains, indicating that it may be a useful technique for polycrystalline materials in general. High throughput image analysis and EBSD now make the necessary sample sizes practical. We illustrate by applying the method to a basaltic rock specimen.

I. INTRODUCTION

An optical- or electron-microscopy image of a polycrystalline material typically represents a two-dimensional (2D) section through a complex three-dimensional (3D) geometry. Reconstructing statistics of the 3D structure from these 2D data remains a major challenge since Wicksell [1] first studied the "corpuscle" problem of deducing the size distribution of randomly placed spheres from the circles seen in a planar cross section. Although this simplest of problems is mathematically well posed, solving it for the 3D distribution by direct inversion of the Wicksell integral is numerically challenging [2]. Instead, moment methods, which reconstruct moments of the 3D structure from moments in 2D [1,3], are a more practical method for obtaining useful 3D information, such as average grain sizes and the width of the size distribution.

In metals and ceramics, grains or crystals (which in this contribution we assume to be equivalent) are rarely even approximately spherical, being often strongly triaxial, with all three axes of different length. It may however be a reasonable approximation that they are oriented randomly in space. If all the 3D shapes are known to be identical, it is possible to fit the distribution of aspect ratios of the 2D sections to examples of 3D shapes from a database [4–6]. For the more realistic case of polydisperse crystals, even if we approximate their shapes, for mathematical simplicity, as ellipsoids (Fig. 1), we

are presented with the problem of computing a 3D ellipsoid size and shape distribution from the elliptical outlines obtained in section. For special cases where certain types of orientation can be assumed [7], or where the grains are known to be ellipsoids of revolution [8] (two of the axes are equal), the inversion is mathematically possible. However, for randomly oriented triaxial ellipsoids, this generalized Wicksell problem is ill-posed: more than one 3D size and shape distribution can yield statistically the same population of elliptical sections. This is easy to see from the dimensionality of the data and target; for let $F(A,B,C)\,\delta A\,\delta B\,\delta C$ be the fraction of the number of ellipsoids per unit volume with major axes of lengths A, B, and C, where A is in the range A to $A + \delta A$, and similarly for B and C. The function $F(A,B,C)$ depends on three variables, while the corresponding distribution of ellipse sizes and shapes depends only on the two ellipse axis lengths. Deducing a probability distribution over three independent variables from one over two is in general not possible.

So far we have considered only the shapes and sizes of grains visible on a section. However, electron back-scatter diffraction (EBSD) is a method that provides information about the crystallographic orientation of grains [9,10], usually expressed as a set of Euler angles [11].

In this contribution we show that if the major axes of each grain's shape are aligned with the crystallographic axes of its lattice (see later for a more detailed discussion), the extra data available from EBSD provides enough information to solve most of the Wicksell problem for triaxial ellipsoids. We also show (using synthetic data) that the same analysis works to a good approximation for triaxial cuboids, and so may be useful for grains in general polycrystalline materials whenever the

---

[*]robert.s.farr@gmail.com
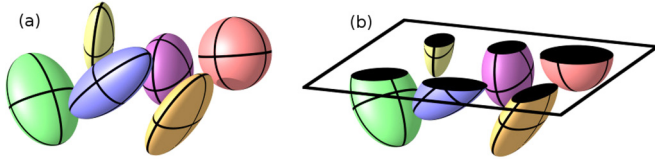[†]zv211@cam.ac.uk
[‡]marian@esc.cam.ac.uk

FIG. 1. (a) A collection of randomly oriented polydisperse ellipsoids. (b) A plane section through the collection produces a set of ellipses (black) from which we wish to reconstruct statistical information about the 3D structure.

crystallographic axes can be assumed to align with the principal axes of the grain shapes.

Specifically, through Eq. (40), we are able to deduce many of the moments of the ellipsoid size and shape distribution from corresponding moments taken from a 2D section. As a simple example of what this information captures, we suggest a set of moment ratios which estimate an average 3D grain size and shape.

Lastly, we show the analysis applied to a real rock section imaged using EBSD. Of particular petrological interest is the distribution of shapes of the mineral plagioclase. Plagioclase forms up to 50 vol. % of rocks of basaltic bulk composition and is commonly an early crystallizing phase. Under the conditions of interface-controlled growth that pertain to most geological environments, plagioclase forms variably elongated tabular facetted grains, with elongation commonly along the c axis, and tablets flattened parallel to the b axis. In basaltic rocks in which the plagioclase is randomly oriented (i.e., those in which the grains have not been rearranged by the action of magmatic currents or by gravitational instability and slumping of a crystal pile) the average grain size and shape carries key information about the cooling and crystallization history [12]. Currently, these data are invariably extracted from 2D sections through the rock. Relating these robustly to 3D grain geometries could shed better light on fundamental processes in rock formation.

II. BACKGROUND: MOMENTS IN 3D AND 2D

A. Calculating moments

Suppose we have a collection of randomly positioned, randomly oriented ellipsoids in space, with N such grains per unit volume. Let $F(A,B,C)$ be the probability distribution, by number, for the polydisperse ellipsoids over their major axis lengths A, B, and C (which we assume to be tied to particular crystallographic directions). Thus F is normalized:

$$\iiint_{O^+} F(A,B,C)\,dA\,dB\,dC = 1, \tag{1}$$

with O^+ being the positive octant of (A,B,C) space; that is to say $0 \leqslant A \leqslant \infty$, $0 \leqslant B \leqslant \infty$, and $0 \leqslant C \leqslant \infty$. The function $F(A,B,C)$ carries all the information about the size and shape of the grains, and any correlation between size and shape.

We can capture information about F through finding various moments of the distribution:

$$M_{\alpha,\beta,\gamma} \equiv \iiint_{O^+} A^\alpha B^\beta C^\gamma\, F(A,B,C)\,dA\,dB\,dC, \tag{2}$$

where the indices α, β, and γ need not be integers. Instead of using an integral, we can calculate each moment by sampling: suppose that in some sufficiently large volume of space there are ν_{3D} grains in total, then we could also write Eq. (2) more simply as

$$M_{\alpha,\beta,\gamma} = \frac{1}{\nu_{3D}} \sum_i A_i^\alpha B_i^\beta C_i^\gamma, \tag{3}$$

where the summation is over grains in space, and grain i has major axes of length A_i, B_i, and C_i.

The moments of F capture a great deal of (indeed in many cases all) the information about the size and shape of the ellipsoids. For example, ratios of moments can be used to calculate average diameters (see Ref. [3] for the case of spheres), or aspect ratios.

Naturally, from a microscopy image, we have no direct access to F, nor to any of the moments $M_{\alpha,\beta,\gamma}$. What we have instead is a collection of elliptical cross sections through grains. Suppose that we have an image that contains a very large number ν_{2D} of grain cross sections, and suppose that the area of the cross section with label j is a_j. We can consider this as a vector area $\mathbf{a}_j \equiv a_j \hat{\mathbf{n}}$, where $\hat{\mathbf{n}}$ is a unit vector perpendicular to the image plane.

In addition to the area, we may also have information about the crystallographic orientation from EBSD. Suppose that the major axes of the 3D ellipsoid (to which the ellipse in question belongs) are aligned respectively in the directions of the orthonormal (unit) vectors $\mathbf{e}_A$, $\mathbf{e}_B$, and $\mathbf{e}_C$. Let us adopt Bunge's convention (see Ref. [11], page 52) for the Euler angles $(\varphi_1, \Phi, \varphi_2)$. We therefore also know the projections of the area $\mathbf{a}_j$ onto the directions of each of the major axes of the ellipsoid:

$$a_{A,j} \equiv a_j\, \hat{\mathbf{n}} \cdot \mathbf{e}_A = a_j \sin \Phi \sin \varphi_2, \tag{4}$$

$$a_{B,j} \equiv a_j\, \hat{\mathbf{n}} \cdot \mathbf{e}_B = -a_j \sin \Phi \cos \varphi_2, \tag{5}$$

$$a_{C,j} \equiv a_j\, \hat{\mathbf{n}} \cdot \mathbf{e}_C = a_j \cos \Phi. \tag{6}$$

These data allow us to calculate any of the 2D moments

$$m_{\alpha,\beta,\gamma} = \frac{1}{\nu_{2d}} \sum_j a_j^4\, |a_{A,j}|^\alpha |a_{B,j}|^\beta |a_{C,j}|^\gamma. \tag{7}$$

In Eq. (7) note that there is an "extra" factor of a_j^4, and also that, once more, the numbers α, β, and γ do not need to be integers.

The key result of this paper (derived below) is that there is a mathematical relation between the 2D moments $m_{\alpha,\beta,\gamma}$ (which can be calculated from microscopy data), and *different* 3D moments $M_{\alpha',\beta',\gamma'}$. This allows 2D microscopy data to be used to directly calculate properties of the 3D ellipsoid distribution. The exact relation is given in Eq. (40).

B. Which moments are useful?

For spheres, one might typically characterize the distribution of sizes through the volume-weighted mean diameter $D_{4,3}$ [3,13] (which is the ratio of the fourth to the third moment of the diameters), or the surface-weighted mean diameter $D_{3,2}$.

Equation (40) shows that for triaxial ellipsoids, not all ratios of moments can be calculated. This is because some of the factorials may diverge, but also because if there is a negative index in $m_{\alpha,\beta,\gamma}$, then for some grain orientations, values of $a_{A,j}$, $a_{B,j}$ or $a_{C,j}$ in Eq. (7) may be close to zero, and so cause numerical problems, even if the overall power of a_j is not problematic. Large moment indices do not have this issue with mathematical divergence; however, they are mostly determined by the largest grains in the sample, and so do not capture the properties of a typical grain, and may furthermore have poor statistics due to the small numbers involved.

Here we suggest that the simplest practical averages for the three major axis lengths are the ratios

$$A_{4,3} \equiv \frac{M_{4,3,4}\, M_{4,4,3}}{M_{3,3,3}\, M_{4,4,4}} \approx 1.231 \left(\frac{m_{0,1,0}\, m_{0,0,1}}{m_{0,0,0}\, m_{\frac{1}{2},\frac{1}{2},\frac{1}{2}}} \right), \quad (8)$$

$$B_{4,3} \equiv \frac{M_{3,4,4}\, M_{4,4,3}}{M_{3,3,3}\, M_{4,4,4}} \approx 1.231 \left(\frac{m_{1,0,0}\, m_{0,0,1}}{m_{0,0,0}\, m_{\frac{1}{2},\frac{1}{2},\frac{1}{2}}} \right), \quad (9)$$

$$C_{4,3} \equiv \frac{M_{3,4,4}\, M_{4,3,4}}{M_{3,3,3}\, M_{4,4,4}} \approx 1.231 \left(\frac{m_{1,0,0}\, m_{0,1,0}}{m_{0,0,0}\, m_{\frac{1}{2},\frac{1}{2},\frac{1}{2}}} \right). \quad (10)$$

These use 3D moments that are as small as possible, without the indices of the corresponding 2D moments being negative. We have used the subscript "4,3" to indicate which 3D moments are involved; however, they are not equivalent to $D_{4,3}$ for spheres, but depend upon substantially higher moments of the population. The high moments mean that these averages depend almost entirely on the larger grains in the distribution, and also means that many grains need to be sampled to achieve good statistics.

We note that with enough grain data, moment ratios might be taken to characterize other properties, such as the width of the polydisperse shape distribution.

III. THEORY: RELATION BETWEEN 3D AND 2D MOMENTS

A. Plane sections through spheres

We begin the derivation with a simple case: suppose that instead of being polydisperse, triaxial ellipsoids, all of the grains in the 3D sample were identical (monodisperse) spheres, all of diameter D_0. As before, let N be the number of grains per unit volume of space. Let us consider sampling this distribution by passing a plane section through it, perpendicular to a unit vector $\hat{\mathbf{n}}$. Whenever a plane section passes through a crystal, it produces an ellipse (in this case always a circle).

The maximum thickness of the sphere in the direction $\hat{\mathbf{n}}$ is of course D_0, so the number of ellipses per unit area of the section is n, where

$$n = N D_0. \quad (11)$$

Let the fraction of the ellipses that have areas between a and $a + \delta a$ be $f_a(a)\delta a$ [so f is normalized in that $\int f_a(a)da = 1$]. Suppose the section lies at a perpendicular distance $r \in (0, D_0/2)$ from the center of a sphere, then we know that the fraction of ellipses that have r in the range r to $r + \delta r$ is simply

$$f_r(r) = 2/D_0. \quad (12)$$

Noting that $f_a(a)|da| = f_r(r)|dr|$ and from Pythagoras' theorem $\pi r^2 + a = \pi D_0^2/4$, we find

$$f_a(a) = \begin{cases} [4a_0(a_0 - a)]^{-1/2} & \text{if } 0 \leqslant a \leqslant a_0, \\ 0 & \text{otherwise,} \end{cases} \quad (13)$$

where $a_0 = \pi D_0^2/4$ is the maximum area of a cross section.

We now make two observations about this formula: First, if we are considering plane sections perpendicular to all possible directions $\hat{\mathbf{n}}$, we can define a vector area of each ellipse as $\mathbf{a} \equiv a\hat{\mathbf{n}}$. Let the fraction of the ellipses that have vector areas in a small region of $\mathbf{a}$-space $\delta \mathbf{a}$ around $\mathbf{a}$ be $f(\mathbf{a})\delta\mathbf{a}$, and suppose f to be normalized:

$$\iiint f(\mathbf{a})\, d^3\mathbf{a} = 1. \quad (14)$$

Then f and f_a are related through

$$f_a(a) = 4\pi a^2 f(\mathbf{a}). \quad (15)$$

Second, suppose we are once again considering the ellipses that lie perpendicular to a specific direction $\hat{\mathbf{n}}$, but that all the spheres have been deformed into ellipsoids by stretching or compressing in the two directions perpendicular to $\hat{\mathbf{n}}$, so that $\hat{\mathbf{n}}$ is the direction of one of the principal axes (which remains unchanged by this deformation). We suppose the deformation to be the same for all ellipsoids, then a_0 takes a new value, but the thickness D_0 of the ellipsoid is unchanged. We observe that, despite this change, both Eqs. (11) and (13) still apply (the latter with the new value of a_0.)

B. Affine transformation of ellipsoids

Consider a general ellipsoid, which in Cartesian coordinates (x,y,z) is represented by the equation

$$\mathbf{r}^T \underline{\underline{A}}\, \mathbf{r} = 1, \quad (16)$$

where

$$\mathbf{r} \equiv \begin{pmatrix} x \\ y \\ z \end{pmatrix} \quad \text{and} \quad \underline{\underline{A}} \equiv \begin{pmatrix} A_{11} & A_{12} & A_{13} \\ A_{12} & A_{22} & A_{23} \\ A_{13} & A_{23} & A_{33} \end{pmatrix}. \quad (17)$$

Suppose that there are N of these ellipsoids per unit volume of space, all identical, and identically oriented, but placed randomly without overlapping. Imagine that we are interested in taking a cross section through this distribution perpendicular to the $\hat{\mathbf{n}}$ direction, which we take for the present to be the Cartesian z-coordinate direction.

Now, whatever the distribution of elliptical cross sections may be for this set of ellipsoids, it must be unchanged by applying an affine transformation to space consisting of a simple shear which moves points only perpendicular to the z direction. In other words, we must obtain the same distribution for ellipse areas (provided $\hat{\mathbf{n}}$ is fixed) if we make the transformation $\mathbf{r} \mapsto \mathbf{r}'$, where

$$\mathbf{r} = \begin{pmatrix} 1 & 0 & p \\ 0 & 1 & q \\ 0 & 0 & 1 \end{pmatrix} \mathbf{r}' \quad (18)$$

for any real numbers p and q, and consider the transformed ellipsoid in $\mathbf{r}'$ space. Choosing the special values

$p = (A_{23}A_{12} - A_{22}A_{13})/(A_{11}A_{22} - A_{12}^2)$ and $q = (A_{13}A_{12} - A_{11}A_{23})/(A_{11}A_{22} - A_{12}^2)$ leads to a new equation for the ellipsoid in the transformed space:

$$(\mathbf{r}')^T \begin{pmatrix} A_{11} & A_{12} & 0 \\ A_{12} & A_{22} & 0 \\ 0 & 0 & \det \underline{\underline{A}}/(A_{11}A_{22} - A_{12}^2) \end{pmatrix} \mathbf{r}' = 1. \quad (19)$$

This describes an ellipsoid which has one of its major axes aligned in the z' direction, and we wish to know two things: First, the length D_0 of this major axis, because for the untransformed ellipsoid, this is the widest separation of two planes (both perpendicular to $\hat{\mathbf{n}}$) which intersect the ellipsoid. Second, we wish to know the maximum cross-sectional area a_0 of the transformed ellipsoid perpendicular to the z' direction (which is also the maximum cross-sectional area of the untransformed ellipsoid perpendicular to the z direction). These quantities can be read directly from Eq. (19), but it is useful to have them in coordinate-independent form. To aid this, we define a new matrix

$$\underline{\underline{B}} \equiv \begin{pmatrix} A_{11} & A_{12} & 0 \\ A_{12} & A_{22} & 0 \\ 0 & 0 & 1 \end{pmatrix} = \hat{\mathbf{n}}\hat{\mathbf{n}}^T + (I - \hat{\mathbf{n}}\hat{\mathbf{n}}^T)\underline{\underline{A}}(I - \hat{\mathbf{n}}\hat{\mathbf{n}}^T).$$

$$(20)$$

We then see, from Eqs. (19) and (20), that

$$D_0 = 2\left(\frac{\det \underline{\underline{B}}}{\det \underline{\underline{A}}}\right)^{1/2}, \quad (21)$$

$$a_0 = \frac{\pi}{(\det \underline{\underline{B}})^{1/2}}, \quad (22)$$

which can be used in Eqs. (11) and (13).

C. The distribution of ellipse areas

Suppose we have N ellipsoids per unit volume, all identical, with major axis lengths (A_0, B_0, C_0) and all initially with the same orientation, so that (with $\hat{\delta}$ being the Kronecker delta function)

$$F(A, B, C) = \hat{\delta}(A - A_0)\,\hat{\delta}(B - B_0)\,\hat{\delta}(C - C_0). \quad (23)$$

If we now choose Cartesian coordinate axes in the direction of the major axes of the ellipsoids, and choose the origin at the center of one of them, then the equation for this ellipsoid is

$$\frac{4x^2}{A_0^2} + \frac{4y^2}{B_0^2} + \frac{4z^2}{C_0^2} = 1. \quad (24)$$

Let us take a comprehensive set of plane sections through space. By comprehensive we mean choosing many random orientations $\hat{\mathbf{n}}$ (over the full solid angle of 4π steradians), and for each orientation, densely and uniformly filling space with parallel plane sections perpendicular to this direction. Whenever a plane passes through an ellipsoid, we note the area a of the ellipse formed, so that we can define a vector

$$\mathbf{a} \equiv a\hat{\mathbf{n}} \quad (25)$$

specifying both its area and direction. Averaged over all these plane orientations and positions, we wish to calculate the

number n of ellipses per unit area of cross section, and also the normalized function f, defined such that the fraction of the total number of ellipses that have values of the vector $\mathbf{a}$ within a small neighbourhood $\delta\mathbf{a}$ is $f(\mathbf{a})\delta\mathbf{a}$.

The number of ellipses per unit area in the cross section with vector areas within a region $\delta\mathbf{a}$ around a specific $\mathbf{a}$ is $n\,f(\mathbf{a})\,\delta\mathbf{a}$. Thus from Eqs. (11), (13), and (15),

$$4\pi a^2 n f(\mathbf{a}) = \begin{cases} N D_0 [4a_0(a_0 - a)]^{-1/2} & \text{if } 0 \leqslant a \leqslant a_0, \\ 0 & \text{otherwise.} \end{cases}$$

$$(26)$$

From Eqs. (24), (21), (22), and (20), we find

$$D_0 = \left(A_0^2 n_x^2 + B_0^2 n_y^2 + C_0^2 n_z^2\right)^{1/2}, \quad (27)$$

$$a_0 = \frac{\pi A_0 B_0 C_0}{4\left(A_0^2 n_x^2 + B_0^2 n_y^2 + C_0^2 n_z^2\right)^{1/2}}, \quad (28)$$

so from Eqs. (13), (23), (25), and (26),

$$n f(\mathbf{a}) = \frac{N D_0^{3/2} \pi^{-3/2} 4^{-1} a^{-2}}{(A_0 B_0 C_0)^{1/2} [\pi A_0 B_0 C_0/(4D_0) - a]^{1/2}} \quad (29)$$

for

$$\frac{4\left(A_0^2 a_x^2 + B_0^2 a_y^2 + C_0^2 a_z^2\right)^{1/2}}{\pi A_0 B_0 C_0} < 1 \quad (30)$$

and zero otherwise. Therefore

$$n f(\mathbf{a}) = \iiint_{\Omega'_{\mathbf{A}} \cap O^+} \frac{N F ABC \Delta}{32a^4(1 - \Delta^{1/2})^{1/2}} \, dA\, dB\, dC, \quad (31)$$

where

$$\Delta \equiv \frac{16\left(A^2 a_A^2 + B^2 a_B^2 + C^2 a_C^2\right)}{\pi^2 A^2 B^2 C^2}. \quad (32)$$

In Eq. (32) we have relabeled (a_x, a_y, a_z) as (a_A, a_B, a_C), to emphasize that a_A (for example) is the projection of $\mathbf{a}$ onto the A axis of the ellipsoid it belongs to. Furthermore, $\Omega'_{\mathbf{A}}$ is the region of the space (A, B, C) which, for fixed $\mathbf{a}$, lies *outside* the sextic surface $16(A^2 a_A^2 + B^2 a_B^2 + C^2 a_C^2) = \pi^2 A^2 B^2 C^2$ (the prime being used to indicate the complement of the set $\Omega_{\mathbf{A}}$ which lies *inside* the sextic surface). As above, O^+ is the positive octant of the space (A, B, C).

We make a final observation before completing the calculation: Since the number of ellipses per unit area of plane section and the number of ellipsoids per unit volume both combine in a simple, additive manner when distributions are combined, then provided we always project $\mathbf{a}$ onto the local directions of the major axes of each ellipsoid, Eq. (31) applies equally to a fully polydisperse distribution of ellipsoids with random orientations. The necessity to project $\mathbf{a}$ onto the major axis direction of its ellipsoid is the reason we need the crystallographic orientation data from EBSD.

D. Moments of ellipsoids from moments of ellipses

To obtain the relation between the 2D moments $m_{\alpha,\beta,\gamma}$ of Eq. (7) and the 3D moments $M_{\alpha,\beta,\gamma}$ of Eq. (3), we simply integrate moments of Eq. (31) over all $\mathbf{a}$ space, which needs to be done in several steps. Remembering that n is the number

of elliptical sections per unit area, we find from Eq. (7) and then (31):

$$
\begin{aligned}
n\, m_{\alpha,\beta,\gamma} &\equiv \iiint a^4\, |a_A|^\alpha |a_B|^\beta |a_C|^\gamma\, n\, f(\mathbf{a})\, d^3\mathbf{a} \\
&= \iiint \left\{ \iiint_{\Omega'_A \cap O^+} \left[|a_A|^\alpha |a_B|^\beta |a_C|^\gamma \right.\right. \\
&\quad \left.\left. \times \frac{N\, F\, ABC\, \Delta}{32\sqrt{1-\Delta^{1/2}}} \right] dA\, dB\, dC \right\} d^3\mathbf{a}.
\end{aligned}
\tag{33}
$$

The next step is to reverse the order of integration, giving

$$
\begin{aligned}
n\, m_{\alpha,\beta,\gamma} &= \iiint_{O^+} \left\{ \iiint_{\Omega_\mathbf{a}} \left[|a_A|^\alpha |a_B|^\beta |a_C|^\gamma \right.\right. \\
&\quad \left.\left. \times \frac{N\, F\, ABC\, \Delta}{32\sqrt{1-\Delta^{1/2}}} \right] d^3\mathbf{a} \right\} dA\, dB\, dC.
\end{aligned}
\tag{34}
$$

Note that in Eq. (34) we have introduced a new integration region $\Omega_\mathbf{a}$, which for fixed A, B, and C is the region of $\mathbf{a}$ space that lies *inside* the ellipsoid $16(A^2 a_A^2 + B^2 a_B^2 + C^2 a_C^2) = \pi^2 A^2 B^2 C^2$.

Next, we introduce a change of variables from $\mathbf{a}$ to

$$
\mathbf{x} \equiv (x,y,z) = \left(\frac{4a_A}{\pi BC}, \frac{4a_B}{\pi AC}, \frac{4a_C}{\pi AB} \right),
\tag{35}
$$

to give

$$
\begin{aligned}
n\, m_{\alpha,\beta,\gamma} &= \iiint_{O^+} \left\{ \iiint_{|\mathbf{x}|<1} \left[|x|^\alpha |y|^\beta |z|^\gamma \right.\right. \\
&\quad \left.\left. \times \left(\frac{\pi}{4}\right)^{\alpha+\beta+\gamma+3} \frac{N\, F\, A^{3+\beta+\gamma} B^{3+\alpha+\gamma} C^{3+\alpha+\beta}}{32\sqrt{1-|\mathbf{x}|}} \right] \right.\\
&\quad \left. \times |\mathbf{x}|^2\, d^3\mathbf{x} \right\} dA\, dB\, dC.
\end{aligned}
\tag{36}
$$

We can then use the definition of the 3D moments in Eq. (3) to perform the integral in (A,B,C) space:

$$
\begin{aligned}
n\, m_{\alpha,\beta,\gamma} &= \frac{N}{32}\left(\frac{\pi}{4}\right)^{\alpha+\beta+\gamma+3} M_{\beta+\gamma+3,\alpha+\gamma+3,\alpha+\beta+3} \\
&\quad \times \iiint_{|\mathbf{x}|<1} \frac{|x|^\alpha |y|^\beta |z|^\gamma |\mathbf{x}|^2}{\sqrt{1-|\mathbf{x}|}}\, d^3\mathbf{x}.
\end{aligned}
\tag{37}
$$

The integral over $\mathbf{x}$ space can be performed by a change of variables to spherical polars (r,θ,ϕ):

$$
\begin{aligned}
n\, m_{\alpha,\beta,\gamma} &= \frac{N}{32}\left(\frac{\pi}{4}\right)^{\alpha+\beta+\gamma+3} M_{\beta+\gamma+3,\alpha+\gamma+3,\alpha+\beta+3} \\
&\quad \times \int_{r=0}^1 \frac{r^{\alpha+\beta+\gamma+4}}{\sqrt{1-r}}\, dr \\
&\quad \times \int_{\theta=0}^\pi |\sin\theta|^{\alpha+\beta+1} |\cos\theta|^\gamma\, d\theta \\
&\quad \times \int_{\phi=0}^{2\pi} |\cos\phi|^\alpha |\sin\phi|^\beta\, d\phi
\end{aligned}
\tag{38}
$$

$$
\begin{aligned}
&= \frac{N\sqrt{\pi}}{16}\left(\frac{\pi}{4}\right)^{\alpha+\beta+\gamma+3} M_{\beta+\gamma+3,\alpha+\gamma+3,\alpha+\beta+3} \\
&\quad \times \frac{(\alpha+\beta+\gamma+4)!\left(\frac{\alpha-1}{2}\right)!\left(\frac{\beta-1}{2}\right)!\left(\frac{\gamma-1}{2}\right)!}{\left(\alpha+\beta+\gamma+\frac{9}{2}\right)!\left(\frac{\alpha+\beta+\gamma+1}{2}\right)!}.
\end{aligned}
\tag{39}
$$

Lastly, since we are interested in obtaining values of 3D moments from calculated 2D moments, we can switch around Eq. (39) to read

$$
\begin{aligned}
M_{\alpha,\beta,\gamma} &= \left(\frac{16n}{N\sqrt{\pi}}\right)\left(\frac{4}{\pi}\right)^{\frac{\alpha+\beta+\gamma-3}{2}} \\
&\quad \times m_{\left(\frac{-3-\alpha+\beta+\gamma}{2}\right),\left(\frac{-3+\alpha-\beta+\gamma}{2}\right),\left(\frac{-3+\alpha+\beta-\gamma}{2}\right)} \\
&\quad \times \frac{\left(\frac{\alpha+\beta+\gamma}{2}\right)!}{\left(\frac{\alpha+\beta+\gamma-1}{2}\right)!\left(\frac{-5-\alpha+\beta+\gamma}{4}\right)!} \\
&\quad \times \frac{\left(\frac{\alpha+\beta+\gamma-7}{4}\right)!}{\left(\frac{-5+\alpha-\beta+\gamma}{4}\right)!\left(\frac{-5+\alpha+\beta-\gamma}{4}\right)!}.
\end{aligned}
\tag{40}
$$

Equation (40) is the main result of this paper. We note that although we do not know N, this is no impediment to calculating averages of the crystal sizes and shapes in 3D, since these depend on ratios of moments rather than the moments themselves, so the factor of N cancels out.

IV. SYNTHETIC DATA: HOW MANY GRAINS ARE NEEDED?

A. Synthetic distribution of ellipsoids

As with any moment method, the results above are exact in the limit of infinite sample size. However, it is useful to have some indication as to how many grain cross sections should be measured in order to obtain a required level of accuracy for the estimates of average 3D grain sizes and shapes.

In order to do this, and also test the results above, we generated randomly oriented monodisperse ellipsoids in space (Fig. 2), and accumulated statistics for the various moments $m_{\alpha,\beta,\gamma}$. We note that in order to generate a random orientation for the orthonormal vectors $\mathbf{e}_A$, $\mathbf{e}_B$, and $\mathbf{e}_C$ specifying the directions of the ellipsoid's principal axes, one needs to choose φ_1 and φ_2 to be uniformly distributed on the interval $(0,2\pi)$, but $\cos\Phi$ needs to be uniformly distributed on the interval $(-1,1)$. Figure 3 shows results where we have chosen the major axes of every ellipsoid to have the values $(A,B,C) = (9,3,1)$.

We see that the fractional error in the major axis lengths, which we have estimated using $(A_{4,3}, B_{4,3}, C_{4,3})$ from Eqs. (8) to (10), falls roughly as $5\nu_{2D}^{-1/2}$, where ν_{2D} is the number of grain cross sections used in the estimate.

B. Synthetic distribution of cuboids

Grains in real samples are unlikely to be ellipsoids, so it is interesting to ask whether the moment method developed here can be applied to other grain shapes, and if so, in what sense we should interpret the results?
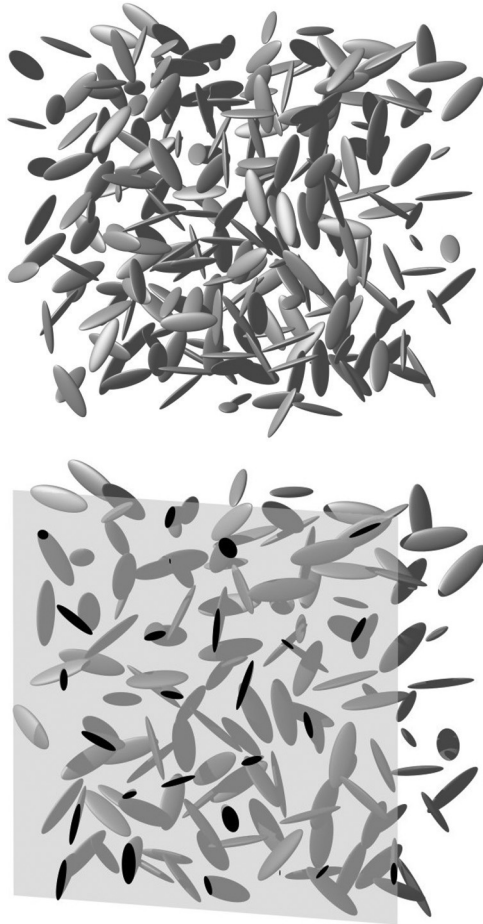
FIG. 2. Top: Random distribution of randomly oriented monodisperse ellipsoids in space. Each ellipsoid has major axes of length $(A_0, B_0, C_0) = (9, 3, 1)$. Bottom: The same distribution cut by a plane, showing (in black) the elliptical cross sections produced.

To this end, we consider synthetic data for cuboids, which are again monodisperse, and placed with random positions and orientations in space (see Fig. 4). We consider a cuboid to be "equivalent" to an ellipsoid if they have the same volume, and if the ratios of edge lengths of the cuboid are the same as the ratios of major axis lengths of the ellipsoid. We therefore choose the edge lengths of the cuboids in the new synthetic data set to be $9(\pi/6)^{1/3}$, $3(\pi/6)^{1/3}$, and $(\pi/6)^{1/3}$, so that the equivalent cuboid has $(A, B, C) = (9, 3, 1)$. We will consider the moment method applied to the cuboids a success, if the calculated estimates $(A_{4,3}, B_{4,3}, C_{4,3})$ are close to the values for the equivalent ellipsoid, namely $(9, 3, 1)$.

Figure 5 shows that the fractional error in the equivalent major axis lengths, which we have estimated using Eqs. (8) to (10), falls roughly as $7\nu_{2D}^{-1/2}$, where ν_{2D} is the number of grain cross sections used in the estimate. For very large values of ν_{2D}, we expect this correlation to break down, and the errors to stop decaying, since there is likely to be a residual, systematic error when naively applying a result for ellipsoids to cuboids. Nevertheless, we propose that $7\nu_{2D}^{-1/2}$ provides a reasonable first estimate of the relative error when applying the moment method here to real samples.
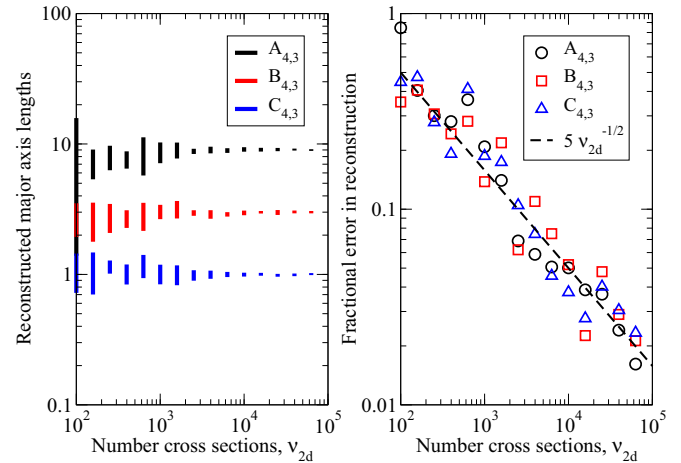

FIG. 3. Reconstructed major axis lengths for monodisperse ellipsoids with major axes $(A_0, B_0, C_0) = (9, 3, 1)$. The vertical bars in the left panel show the range (mean plus or minus one standard deviation) for ten repeats. Right-hand panel shows the fractional error in the reconstructed axis lengths, in the sense of the greatest distance of the standard deviation bar from the true value, divided by the true value. We see that the standard deviation of predictions falls as the number of ellipses ν_{2D} increases. Furthermore, the predictions become more and more accurate in the same limit, with a fractional error falling roughly as $5\nu_{2D}^{-1/2}$.

V. MATERIALS AND METHODS

A. Definitions for real samples

For real-world rock samples, we need to address some definitions, in order for our results to be meaningful. The method here is concerned with the statistics of grains, where each grain is a single crystal, with an atomic lattice whose orientation can be identified with EBSD.

Each grain is considered to be equivalent to a particular ellipsoid, in a sense which we have described so far only for cuboids. For more general grain shapes, we adopt the following definition: Let a grain occupy a set G of points $\mathbf{r}$ in 3D space. Define a symmetric positive-definite tensor

$$g_{ij} \equiv \int_G (r_i - \langle r_i \rangle)(r_j - \langle r_j \rangle) d^3\mathbf{r}. \quad (41)$$

The equivalent ellipsoid which corresponds to this grain has the same volume as the grain, has principal axes aligned with the eigenvectors of g_{ij}, and has major axis lengths proportional to the square roots of the corresponding eigenvalues of g_{ij}.

A critical assumption is that the major axes of the ellipsoid are aligned with the crystallographic axes of the lattice. This assumption is, strictly speaking, only meaningful for orthorhombic, tetragonal, or cubic symmetry groups, which have three orthogonal crystallographic axes. For the hexagonal group, if the grains adhere to the symmetry of the crystal, the ellipsoids will be ellipsoids of revolution, and it will be sufficient for the crystallographic c axis to align with the axis of rotation of the ellipsoid.

In the case of the rock sample studied here, the two minerals analyzed are triclinic (plagioclase; which is a solid solution between anorthite and albite, and in our case, close to the anorthite end of the series) and monoclinic (the pyroxene
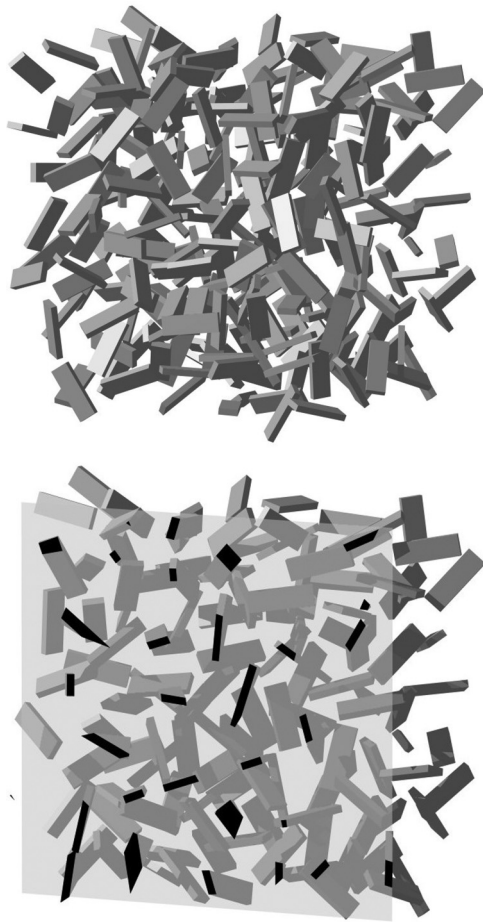
FIG. 4. Top: Random distribution of randomly oriented monodisperse cuboids in space. The equivalent major axes (in the sense defined in the text) are $(A_0, B_0, C_0) = (9, 3, 1)$. Bottom: The same distribution cut by a plane, showing (in black) the polygonal [4] cross sections produced.

augite, which is close to the diopside end-member of a complex solution series). For such crystal systems, care must be exercised in defining an initial orientation to be operated on by the Euler rotations [14]. In this case however, both minerals have crystallographic axes that are not far from being mutually orthogonal: for anorthitic plagioclase, the unit cell angles are [15]: $\alpha = 93.13°$, $\beta = 115.89°$, and $\gamma = 91.24°$; while for diopside [16]: $\alpha = 90°$, $\beta = 105.63°$, and $\gamma = 90°$. Within the uncertainties stated here, we therefore believe that alignment of ellipsoids to crystallographic axes is sufficiently well defined; but we must also ask whether is is likely to be true? For anorthitic plagioclase, which crystallizes first and thus directly from abundant liquid, this alignment assumption is believed to be commonly the case. However, it will be more questionable for late-crystallizing minerals which are forced to accommodate their shapes to interstices between existing grains.

B. Rock sample

The sample we examine is from the Lupchinga dolerite dyke, which belongs to a NNE-trending swarm about 10 km wide and 60 km long, and is exposed on the southern coast of
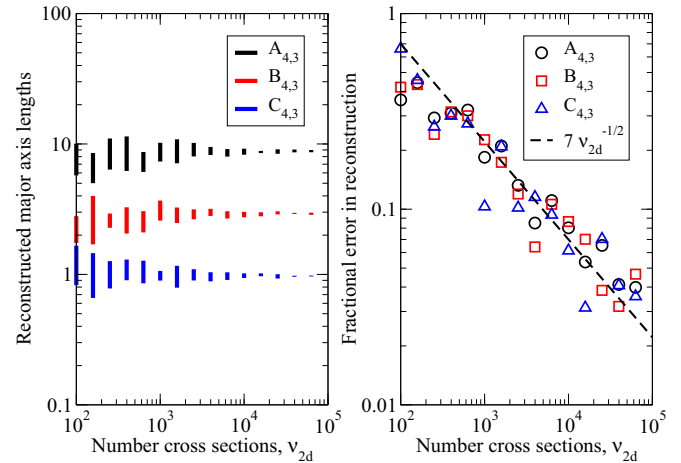

FIG. 5. Reconstructed major axis lengths for monodisperse cuboids with equivalent major axes $(A_0, B_0, C_0) = (9, 3, 1)$. The vertical bars in the left panel show the range (mean plus or minus one standard deviation) for ten repeats. Right-hand panel shows the fractional error in the reconstructed axis lengths, in the sense of the greatest distance of the standard deviation bar from the true value, divided by the true value. We see that the standard deviation of predictions falls as the number of ellipses ν_{2D} increases. Furthermore, the predictions become more and more accurate in the same limit, with a fractional error falling roughly as $7\nu_{2D}^{-1/2}$. We expect that for very large ν_{2D} the errors would eventually cease to fall further.

Lupchinga Island in Pääjärvi Lake, Karelia, NW Russia, where it is 22.4 m wide (it is inaccurately described as 21 m wide in Ref. [17]: R. Latypov, private communication, 2016). We examined a sample collected 6.05 m from the eastern margin. The bulk geochemical composition of this sample is reported in Ref. [17] (their sample number 1/36). The composition of the dyke is generally uniform (with MgO concentration approximately 5.5 wt. %) with a compositionally distinct chilled margin (only the eastern margin is accessible as the western margin is covered by the sea) with MgO increasing to 5.8 wt. %. No phenocrysts (crystals carried by the magma from its source, identifiable by their abnormally large size) are present in the dyke.
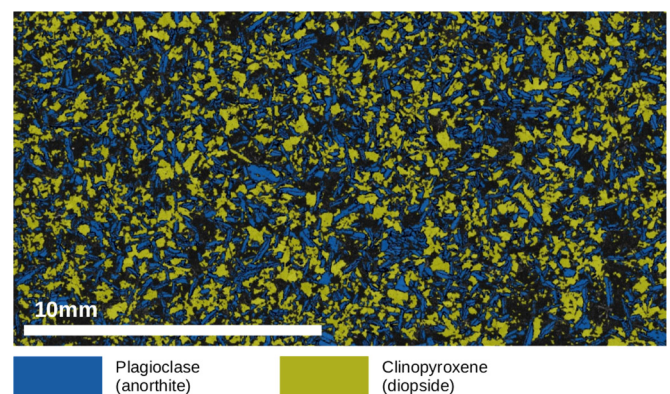

FIG. 6. Image of basaltic rock sample, segmented by mineral type. We apply the analysis here separately to the plagioclase and clinopyroxene grains.

TABLE I. Some of the individual grain data for anorthite from a basaltic rock sample. Note that the four rightmost columns are calculated from data in the other columns, using Eqs. (4) to (6). The data for φ_1 are not needed for these calculations.

Grain no.	Area/μm^2	φ_1	Φ	φ_2	a_j^4/m^8	$|a_{A,j}|$/m^2	$|a_{B,j}|$/m^2	$|a_{C,j}|$/m^2
1	8 099	157.72°	136.23°	295.91°	4.303×10^{-33}	5.040×10^{-9}	2.448×10^{-9}	5.849×10^{-9}
2	20 250	292.65°	130.12°	284.24°	1.681×10^{-31}	1.501×10^{-8}	3.809×10^{-9}	1.305×10^{-8}
⋮	⋮	⋮	⋮	⋮	⋮	⋮	⋮	⋮
3299	4 950	35.99°	65.84°	145.48°	6.004×10^{-34}	2.559×10^{-9}	3.721×10^{-9}	2.026×10^{-9}

C. Electron back-scatter diffraction imaging

After standard mechanical polishing using diamond paste down to 1/4 micron grit size, a 30 μm thick section of rock was polished for 1 h with 0.06 μm colloidal silica (SiO$_2$ particle dispersion in an alkaline solution) at Cambridge University, UK. The sample was analyzed on a FEI sFEG XL30 SEM at the Department of Physics, University of Cambridge. All crystallographic data sets were collected, indexed, and analyzed using Oxford Instruments AZtec acquisition software, set to detect 7 bands, 60 Hough transform, 75 reflectors, at 4 × 4 binning, and 2.7 s time per frame. A whole thin section EBSD was carried out using 15 μm step size, over an area of approximately 20 × 15 mm. Acquisition of the data for the EBSD map took 150 min and the data was processed by Oxford Instrument Channel 5 software.

Channel 5 software permits the construction of maps of mineral phases, shape of grain intersections, and textural component maps. The phase map is determined using the crystallographic matching units of each constitutive phase (for plagioclase we used the matching unit from Angel *et al.* [15], while for clinopyroxene we used the AZtec Dioside.cry reference file [16]).

VI. RESULTS: ANALYSIS OF ROCK SECTION

Figure 6 shows an image of the rock sample, segmented into grains of diopside and anorthite. We perform a moment analysis of the two highlighted mineral types. Table I shows data and calculations applied to a few of the anorthite grains

to illustrate the calculation, and Table II shows the relevant calculated moments for the two grain populations.

The grains of anorthitic plagioclase are seen to have a mean shape which is elongated in the *C*-axis direction and somewhat flattened in the *B*-axis direction. This ordering $B < A < C$ of major axis lengths is expected for interface-controlled growth of plagioclase, and the method presented here has allowed a quantitative, 3D measurement of this anisotropy to be obtained. The shapes of clinopyroxene grains have been less studied in the literature, and we believe these data represent the first statistical analysis of their 3D geometry in a rock sample.

VII. CONCLUSIONS

Automated EBSD mapping of material samples has become a fast and powerful method in recent years, generating large volumes of data. Image analysis can be brought to bear to segment the orientation maps so obtained, and these data sets are ideally suited to the application of moment-based methods for structure characterization.

We believe that the method presented here gives unique structural insight into the 3D nature of polycrystalline samples, provided it can be assumed that the structure is statistically isotropic. Although we have derived the equations for the mathematically ideal case of ellipsoids, the fact that the method also gives accurate results for synthetic data generated for cuboids suggests that it may be generally applicable to the less ideal grain shapes encountered in real samples, provided the results are interpreted as describing equivalent ellipsoids. Here equivalent means having the same volume and ratios of major axis lengths.

Lastly, the estimated accuracy of the results is notable: because we are constrained to moderately large moments, the method gives information mostly about the bigger grains in a polydisperse population. Because of the scarcity of big grains, the method needs a relatively large sample size: to obtain an average shape for the 3D grains to an accuracy of better than 10% requires on the order of 5000 grain sections to be analyzed. This is now within the capabilities of modern EBSD implementations, so we believe the moment method described here is a timely addition to the analysis tools available for electron microscopy.

TABLE II. Grain numbers and 2D moments for mineral populations, and calculated values of average major axis lengths, using Eqs. (8) to (10). Relative errors for $A_{4,3}$, $B_{4,3}$, and $C_{4,3}$ are estimated from $7\nu_{2D}^{-1/2}$.

	Anorthite	Diopside
ν_{2D}	3299	4303
$m_{0,0,0}$/m^8	4.41×10^{-29}	1.17×10^{-29}
$m_{\frac{1}{2},\frac{1}{2},\frac{1}{2}}$/m^{11}	3.66×10^{-39}	3.29×10^{-40}
$m_{1,0,0}$/m^{10}	7.81×10^{-36}	1.52×10^{-36}
$m_{0,1,0}$/m^{10}	1.51×10^{-35}	1.22×10^{-36}
$m_{0,0,1}$/m^{10}	5.12×10^{-36}	8.73×10^{-37}
$A_{4,3}$/μm	590 ± 70	340 ± 40
$B_{4,3}$/μm	300 ± 40	420 ± 50
$C_{4,3}$/μm	900 ± 110	590 ± 60

[1] S. D. Wicksell, The corpuscle problem, a mathematical study of a biometric problem, Biometrika **17**, 84 (1925).

[2] R. S. Anderssen and A. J. Jakeman, Abel type integral equations in stereology. II. Computational methods of solution and the random spheres approximation, J. Microsc. **105**, 135 (1975).

[3] R. S. Farr, V. C. Honour, and M. B. Holness, Mean grain diameters from thin sections: Matching the average to the problem, Mineral. Mag. **81**, 515 (2017).

[4] M. D. Higgins, Numerical modelling of crystal shapes in thin sections: estimation of crystal habit and true size, Am. Mineral. **79**, 113 (1994).

[5] M. D. Higgins, Measurement of crystal size distributions, Am. Mineral. **85**, 1105 (2000).

[6] D. J. Morgan and D. A. Jerram, On estimating crystal shape for crystal size distribution analysis, J. Volcanol. Geotherm. Res. **154**, 1 (2006).

[7] M. A. Przystupa, Estimation of true size distribution of partially aligned same-shape ellipsoidal particles, Scr. Mater. **37**, 1701 (1997).

[8] R. T. De Hoff, The determination of the size distribution of ellipsoidal particles from measurements on random plane sections, Trans. A.I.M.E. **224**, 474 (1962).

[9] A. J. Wilkinson and P. B. Hirsch, Electron diffraction based techniques in scanning electron microscopy of bulk materials, Micron **28**, 279 (1997).

[10] F. J. Humphreys, Grain and subgrain characterisation by electron backscatter diffraction, J. Mater. Sci. **36**, 3833 (2001).

[11] W. Zhou and Z. L. Wang, Eds., *Scanning Microscopy for Nanotechnology: Techniques and Applications* (Springer, New York, 2007), pp. 41–75.

[12] M. B. Holness, The effect of crystallization time on plagioclase grain shape in dolerites, Contrib. Min. Petrol. **168**, 1076 (2014).

[13] D. J. McClements, *Food Emulsions, Principles, Practices and Techniques* (CRC, Taylor Francis, London, 2016), pp. 627–646.

[14] G. Noltze, Euler angles and crystal symmetry, Cryst. Res. Technol. **50**, 188 (2015).

[15] R. J. Angel, M. A. Carpenter and L. W. Finger, Structural variation associated with compositional variation and order-disorder behavior in the anorthite-rich feldspars, Am. Mineral. **75**, 150 (1990).

[16] Diopside.cry from the HLK Oxford Instruments internal database.

[17] S. Chistyakova and R. Latypov, Magma differentiation and crystallization in basaltic conduits by two competing petrogenetic processes, Lithos **148**, 142 (2012).